Geochemical Journal, Vol. 46, pp. 393 to 407, 2012

Sm–Nd geochronology, REE geochemistry and C and O isotope characteristics of calcites and stibnites from the Banian antimony deposit, Guizhou Province, China

JIASHENG WANG,[1,2] HANJIE WEN,[2]* HAIFENG FAN[2] and JINGJING ZHU[2]

[1]Kunming University of Science and Technology, Southwest Institute of Geological Survey, Kunming 650093, China
[2]State Key Laboratory of Ore Deposit Geochemistry, Institute of Geochemistry, Chinese Academy of Sciences, Guiyang 550002, China

(*Received March 21, 2012; Accepted June 22, 2012*)

The Banian sediment-hosted antimony deposit is a medium-sized deposit located in the Dushan County, South Guizhou, China. Calcite is the dominant gangue mineral and can be divided into two types: white and pink. Pink calcite is intimately associated with mineralization. Sm–Nd dating of five white calcites yield an isochron age of 128.2 ± 3.2 Ma, with initial ε_{Nd} = –4.3 and MSWD = 0.54, while six pink calcites yield an identical age of 126.4 ± 2.7 Ma with initial ε_{Nd} = –6.0 and MSWD = 0.68. These new age constraints suggest that the Banian deposit formed during the late Yanshanian.

Negative initial ε_{Nd} values, C (–0.5 to –1.8), O (12.5 to 14.6) isotopic characteristics of calcites, and field observations of abundance of vuggy open spaces, all suggest significant interaction between fluid and wall rocks. Calcites are characterized by strongly LREE-depleted and MREE- and HREE-enriched (LREE/HREE = 0.11–0.61). Stibnites are LREE-enriched, and MREE- and HREE-depleted (LREE/HREE = 105–500). Wall rocks are characterized by moderate LREE-enriched (LREE/HREE = 6.2–12). Pink calcites are more enriched in LREE (LREE/HREE = 0.11–0.61) than white calcites (LREE/HREE = 0.11–0.23), while the concentration of HREE remains nearly constant in both. The high contents of Fe and Mn in calcites and the negative correlation between Fe+Mn (ppm) and LREE/HREE ratios suggest that the Fe–Mn impurities in calcites may dominate the enrichment of MREE and HREE in calcites from the Banian deposit.

Keywords: Banian antimony deposit, calcite, stibnite, Sm–Nd geochronology, REE

INTRODUCTION

Antimony is one of the dominant metals produced in China, accounting for approximately 70% of the world reserves (Peng and Hu, 2001). The antimony deposits are part of a large-scale, low-temperature epithermal metallogenic domain in SW China called the "South China antimony ore belt" (Fig. 1A). The belt is nearly 1900 km long, 200 km wide, and extends from Yunnan in the southwest, to Anhui. The belt contains approximately 500 deposits and occurrences, accounting for about 83% of the total antimony reserves of China (Xiao *et al*., 1992). The Xikuangshan deposit, located in the center of the belt is the largest antimony deposit in the world (Peng *et al*., 2003a). The belt also contains major deposits or ore fields at Muli, Qinglong, Dachang and Dushan.

Despite numerous geological studies (e.g., Xiao *et al*., 1992; Cui *et al*., 1993; Cui and Jin, 1993; Peng and Hu, 2001), a full understanding of the geodynamical setting, fluid evolution, and genesis of the epithermal antimony mineralization has been seriously hampered. Similar to other epithermal deposits (including Au, Hg, As and Tl) in southwestern China, the ore-forming ages of antimony deposits are poorly constrained due to the absence of minerals suitable for isotopic dating and the absence of ore-related intrusions in or near these deposits.

According to mineral composition of ores and genesis, antimony deposits are subdivided into epithermal (e.g., Xikuangshan and Qinglong, China; Ashat, Roundnjany) and metamorphogene-hydrothermal (Woxi, China; La Lucette, France; Gravelot, South Africa) (Obolensky *et al*., 2007), and they are usually hosted within black shales or limestones (Williams-Jones and Norman, 1997; An and Zhu, 2010). The Sb-rich sedimentary rocks and metasedimentary rocks from Precambrian and palaeozoic constitute a possible source of Sb (Peng *et al*., 2003a; Fan *et al*., 2004; Peng and Frei, 2004). The speciation of antimony is known over a considerable range in temperature and fluid composition. Mixed hydroxy–chloride complexes ($Sb(OH)_2Cl^0$, $Sb(OH)_3Cl^-$) control antimony transport in saline high-temperature ore fluids

*Corresponding author (e-mail: wenhanjie@vip.gyig.ac.cn)

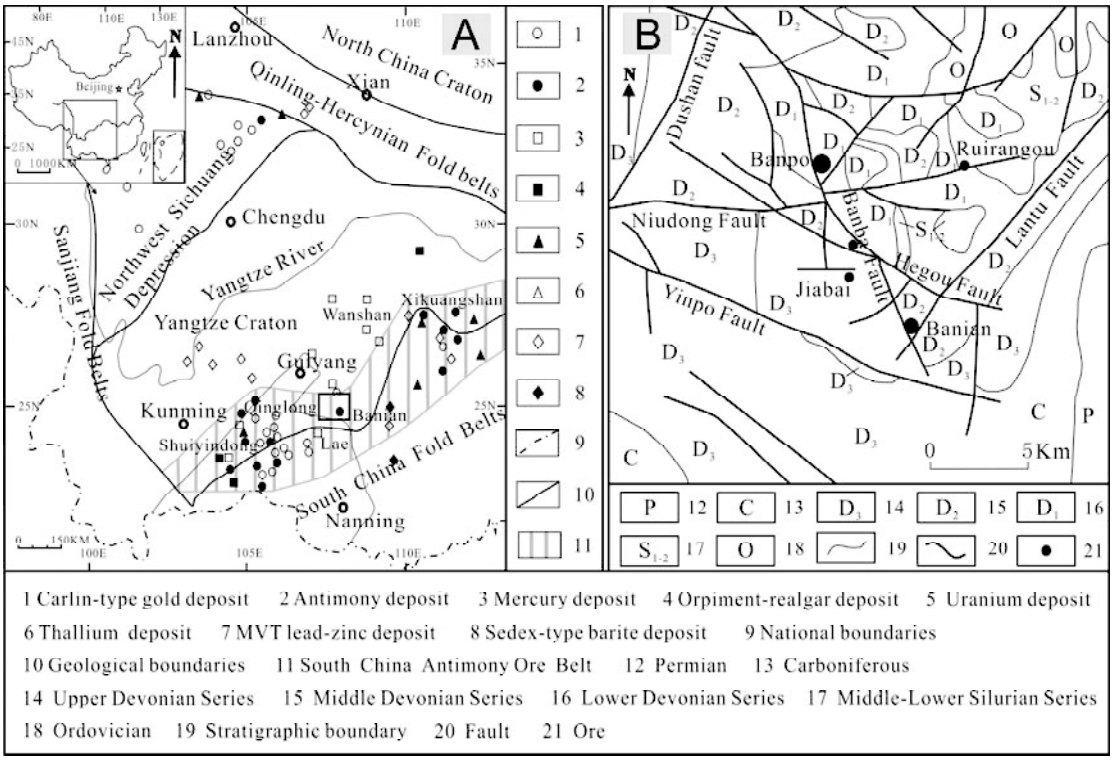

Fig. 1. A) Location map showing the South China antimony ore belt and other epithermal ore deposits in SW China. B) Location of the Banian deposit in the Dushan antimony ore field (after Hu et al., 2002 and Jin and Dai, 2007).

at acidic conditions (Pokrovski *et al*., 2006). However, Antimony hydroxychloride complexes are minor in the neutral low- to moderate-temperature solutions (≤250–300°C) typical of Sb deposits formation; the antimony speciation in these systems is dominated by $Sb(OH)_3$ and Sb–sulfide species ($H_2Sb_2S_4^0$, $HSb_2S_4^-$, $Sb_2S_4^{2-}$) (Krupp, 1988; Pokrovski *et al*., 2006). Stibnite deposition is controlled mainly by temperature decrease and reduction except under alkaline conditions where acidification is the principal cause of mineralization (Williams-Jones and Norman, 1997).

Banian antimony deposit is a medium-sized deposit that forms part of the Dushan antimony ore field in the western part of the South China Antimony Ore Belt (Fig. 1B). It was formed from the fluids of meteoric origin, at average homogenization temperatures of 145°C, salinities ranging from 5.7 to 8.7 wt% equivalent NaCl, based on the fluid inclusions and hydrogen and oxygen isotopes studies (Cui *et al*., 1993; Wang and Jin, 2010). However, only a few C, H, O, S data existed (Cui and Jin, 1993), and its ore-forming age has not been reported until now. Fluorite and quartz are the primary gangue minerals of the nearby large-size Qinglong and Banpo antimony deposits, respectively. At the Banian deposit, calcite is the predominant gangue mineral. Previous studies suggested that stibnite and calcite were formed during the same hydrothermal event (Cui *et al*., 1993).

In recent years, hydrothermal minerals such as fluorite, scheelite, tourmaline and calcite have been successfully used to determine Sm–Nd ages for gold (Bell *et al*., 1989; Anglin *et al*., 1996; Turner *et al*., 2003; Roberts *et al*., 2006; Su *et al*., 2009), tungsten (Darbyshire *et al*., 1996; Eichhorn *et al*., 1997), antimony (Peng *et al*., 2003a, 2003b), other hydrothermal deposits (Halliday *et al*., 1990; Chesley *et al*., 1991, 1994; Jiang *et al*., 2000) and fluid-flow event (Uysal *et al*., 2007). These minerals are ideal for Sm–Nd dating because they usually contain high amounts of Sm and Nd, and display enrichment of MREE and HREE, corresponding to a large variation in Sm/Nd ratios. As a result, the mechanism of LREE/HREE fractionation of hydrothermal Ca-bearing minerals becomes a considerable scientific interest, and remains controversial (Möller *et al*., 1976; Morgan and Wandless, 1980; Chesley *et al*., 1991; Bau and Möller, 1992; Peng *et al*., 2004; Schönenberger *et al*., 2008). Generally, carbonate shows LREE-enriched, low Sm/Nd ratio and in narrow range (0.1–0.3) (Graf, 1984). Nevertheless, a few calcites show MREE- and HREE-enriched, higher Sm/Nd ratio and wider range (0.1–9) (Peng *et al*., 2003a; Uysal *et al*., 2007; Su *et al*., 2009).

This paper presents the results of a study on rare earth element (REE), Fe, Mn and Mg abundances, stable carbon and oxygen isotope compositions, and Sm–Nd geochronology of several stages of calcites and REE characteristics of stibnite from the Banian antimony deposit. Mg, Fe and Mn abundances of LREE-enriched calcites from the Wanshan and Lae mercury deposits are reported for purpose of comparison. The goal of this study is to constrain the timing of ore formation, the origin and evolution of hydrothermal fluids involved in the formation of epithermal antimony mineralization and to illuminate the key factors controlling the enrichment of MREE and HREE in calcites.

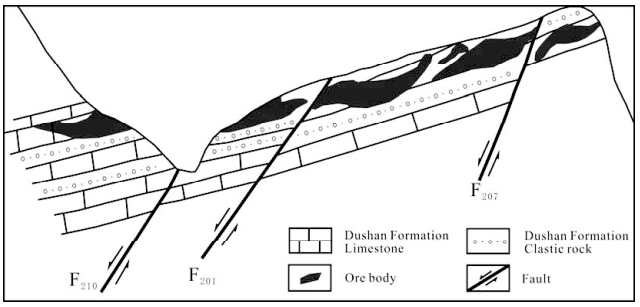

Fig. 2. The sketch map of geological section of the Banian antimony deposit (modified from Cui et al., 1993).

GEOLOGICAL SETTING

The Banian antimony deposit is located in the southeastern area of Dushan County, Guizhou province, China, and is one of the important deposits of the Dushan antimony ore field. Structurally, it is situated in the southwest margin of the South China Fold Belt, and near the southern axial portion of the Dushan box-shaped anticline. The Dushan ore field is mainly controlled by fault fractures, and folds are less developed. The faults can be divided into four major trends oriented NNE, WNW, NNW and EN, respectively. The basal tectonic frame in the region was formed in the Yanshanian orogeny (190–65 Ma) (Cui and Jin, 1993), an important tectonic event in China (Hu *et al*., 2002, 2007a; Peng *et al*., 2003a; Su *et al*., 2009), with widespread tectonism and magmatism that led to large-scale metal mineralization including W, Sn, Pb, Zn, Nb and Ta in SE China and Au, Sb, As, Tl and Hg in SW China (Chen, 1992; Hu *et al*., 2007a). The exposed country rocks mainly consist of Ordovician, Silurian, Devonian, Carboniferous and Permian strata. No igneous rocks crop out in the region. The Banian deposit is mainly controlled by the Banba fault and the secondary Dayuhe fault, and is hosted in the Dushan Formation of Middle Devonian age (Fig. 1B).

The Dushan Formation predominantly consists of shallow marine carbonate and clastic rocks. Based upon variations in lithology, it can be roughly divided into Jipao, Songjiaqiao and Jiwozhai members from the bottom up. All of which are enriched in fossils of coral and brachiopoda. The Songjiaqiao member, based on the different lithological assemblages, can be subdivided into two sub-members: the lower sub-member is characterized by moderate to thick layer of medium-grained quartz sandstone, interlayered with thin beds of argillaceous limestone or limestone; the upper sub-member is characterized by carbonates interbeded with clastic rocks and is the major ore-bearing formation of the Banian deposit (Cui and Jin, 1993).

The orebodies in the Banian deposit usually occur as stratabound or lenticular bodies at the contact between carbonate rocks and clastic rocks, or in interformational sliding and structural breccias. They are parallel to bedding or transgress layering at a slight angle (Fig. 2).

Hydrothermal alteration typically consists of calcification, silicification and sulfidation. The ores are very simple in composition; calcite is the predominant gangue mineral with minor amounts of quartz, pyrite and dolomite. Based on the field and microscopic observations, the calcites can be classified into two types; pink and white. The paragenetic order of these major minerals is white calcite followed by pink calcite and then stibnite. The white calcite is larger in crystal size (5 to 50 mm), and has no direct relationship with mineralization (Fig. 3A). Pink calcite usually occurs in veinlets, veins and as matrix in mineralized breccias ranges in size from 2 to 10 mm and is intimately related to mineralization. Stibnites are 2 to 40 mm in size and generally occur as tabular, prismatical, acicular or radial crystals in pink calcite (Figs. 3A and B) and in surrounding limestone (Fig. 3C). Stibnites has been observed occupying cracks and cleavages of pink calcites, crosscutting calcites, and truncating cleavages in calcites (Fig. 3D). Additionally, near-ore wall rocks are characterized by containing a large quantity of vuggy open space of variable size (<60 mm) (Fig. 3C).

SAMPLING AND ANALYTICAL METHODS

The two types of calcites occurring with stibnites were hand picked and crushed to 40–60 mesh, separately. Mineral splits were then washed in ultrapure water several times, dried at low-temperature (<60°C), and then clean calcite and stibnite separates were handpicked to a purity of more than 99% under a binocular microscope, and ground to 200 mesh in an agate mortar.

Sm–Nd isotopic analytical procedure

Sm and Nd isotope measurements were carried out at

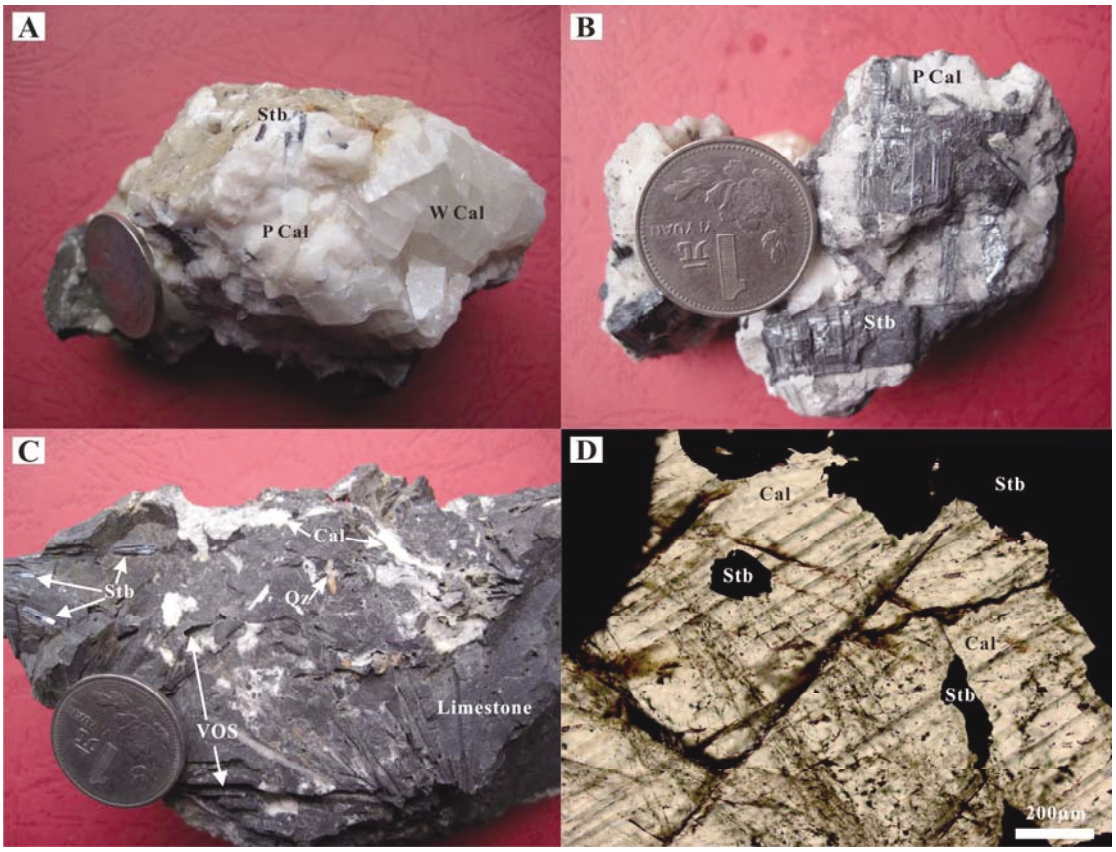

Fig. 3. A) Photograph of stibnites, white and pink calcites, showing the close relationship between pink calcites and stibnites; B) Photograph shows stibnites occur as tabular and prismatical in pink calcites; C) Photograph of slightly altered limestone wall rocks with stibnites and a lot of holes; D) Microphotograph (transmitted light) shows stibnites crosscut the cleavages of pink calcites or grow along its cracks and cleavages. Stb = stibnite; W Cal = white calcite; P Cal = pink calcite; Cal = calcite; Qz = quartz; VOS = vuggy open space.

the Tianjin Institute of Geology and Mineral Resources, CAGS, and analyzed on a mass spectrometer TRITON. The analytical procedure followed, is as described in Peng *et al*. (2003a) and Su *et al*. (2009). Samples were dissolved in Teflon vessels with a mixture of HF and $HClO_4$, at 150°C, for at least 12 hour. Two sample aliquots, each weighting 150 mg were dissolved, one for Sm and Nd concentration measurement and the other for $^{143}Nd/^{144}Nd$ analysis. To separate Sm and Nd, a reverse-phase extraction technique was done with di (2-ethylhexyl) phosphoric acid (HDEHP) coated Teflon powder. Sm and Nd concentrations were determined by isotope dilution using ^{149}Sm–^{146}Nd spike solution. The concentrations of National Primary Standard (GBS04419) and international standard (BCR-1) determined in this study were: Sm = 3.02 ppm, Nd = 10.07 ppm, with $^{143}Nd/^{144}Nd = 0.512739 \pm 5$ (2σ), and Sm = 6.57 ppm, Nd = 28.75 ppm, with $^{143}Nd/^{144}Nd = 0.512644 \pm 5$ (2σ), respectively. Nd ratios were normalized to $^{146}Nd/^{144}Nd$ ratio of 0.7219. The reproducibility of the isotopic ratios is better than 0.005% (2σ); the precision for Sm and Nd concentrations is less than 0.5% of the quoted values (2σ). Total procedure blanks for Sm and Nd were 30 pg and 54 pg, respectively. The replicate analyses of JMC Nd standard (the Johnson and Mattey® Nd standard) gave an average $^{143}Nd/^{144}Nd$ value of 0.511132 ± 5 (2σ). The decay constant used in the age calculation is $\lambda^{147}Sm = 6.54 \times 10^{-12}$/yr. The Sm–Nd isochron ages were calculated with the ISOPLOT 3.23 computer program (Ludwig, 2005).

C and O isotopic analytical procedure

Carbon ($\delta^{13}C$) and oxygen ($\delta^{18}O$) isotopic compositions ($\delta^{18}O$ is referred to SMOW) were analyzed in eight calcite samples (4 white and 4 pink) and one slightly altered limestone sample, following the method of McCrea (1950). In brief, samples were reacted with 100% H_3PO_4 at 25°C for 24 hour. The liberated CO_2 was analyzed using Finnigan MAT 252 mass spectrometer, at the Institute of Geochemistry, Chinese Academy of Sciences, Guiyang. C and O isotopic compositions are reported rela-

Table. 1. Sm and Nd isotopic compositions of calcites from the Banian deposit

Sample No.	Sample characteristic	Sm (ppm)	Nd (ppm)	$^{147}Sm/^{144}Nd$	$^{143}Nd/^{144}Nd$ (2σ)
BN-6-1	White - transparent	0.5528	0.4220	0.7919	0.512912 ± 5
BN-11	White	0.4281	0.4938	0.5242	0.51269 ± 6
BN-14	Transparent	0.3045	0.2021	0.9109	0.513011 ± 12
BN-21	White	0.4492	0.7057	0.3849	0.512565 ± 12
BN-26-1	White - transparent	0.5916	0.5668	0.6309	0.512778 ± 10
BN-9-2	Light pink	0.4740	0.9797	0.2925	0.512411 ± 15
BN-17	Light pink	0.4303	0.5513	0.4718	0.512558 ± 8
BN-22	Light pink	0.5323	0.4595	0.7003	0.512738 ± 10
BN-23	Pink	0.5787	0.3375	1.0366	0.513026 ± 8
BN-26-2	Light pink	0.1496	0.1453	0.6222	0.512681 ± 13
BN-27	Light pink	0.5722	0.5419	0.6383	0.512694 ± 5

tive to PDB and SMOW, respectively. The analytical uncertainty is ±0.2‰.

REE, Fe, Mn and Mg analytical procedure

In order to illustrate the cause of fractionation between LREE and HREE, the Fe, Mn and Mg abundances of LREE-enriched calcites from the Wanshan and Lae mercury deposits in the region were analyzed contemporaneously.

The rare earth elements (REE), Fe, Mn and Mg composition of calcites, stibnites and limestones were all analyzed separately by ALS Minerals—ALS Chemex (Guangzhou) Co., Ltd. For REE analysis, samples were mixed with a flux of lithium borate ($LiBO_2$) and melted in the furnace at 1000°C. When the melt was cooled down, a constant volume of nitric acid was added, and the solution was analyzed with a PerkinElmer ELAN 6000 Inductively Coupled Plasma Quadrupole Mass Spectrometer (ICP-MS). The analytical error is smaller than 10%. The analyses of Fe, Mn and Mg compositions were carried out by digesting 0.4 g of calcite sample with a mixture of nitric acid, perchloric acid, hydrofluoric acid and hydrochloric acid (HNO_3–$HClO_4$–HF–HCl), and then reduced over heat to near-dryness. After adding a constant volume of hydrochloric acid, the sample solution was analyzed with a Varian ICP735-ES Inductively Coupled Plasma Emission Spectroscopy (ICP-AES). The results, corrected for spectrum interferences, are presented in table 3 and 4. The analytical error is smaller than 10%.

RESULT

Sm–Nd isochron age

All the Sm and Nd contents and isotopic values are listed in Table 1, and shown in Fig. 4. Though the contents of Sm (0.1496–0.5916 ppm) and Nd (0.1453–0.9797 ppm) are relatively low in all of the calcite samples, the $^{147}Sm/^{144}Nd$ ratios are highly variable and will result in a

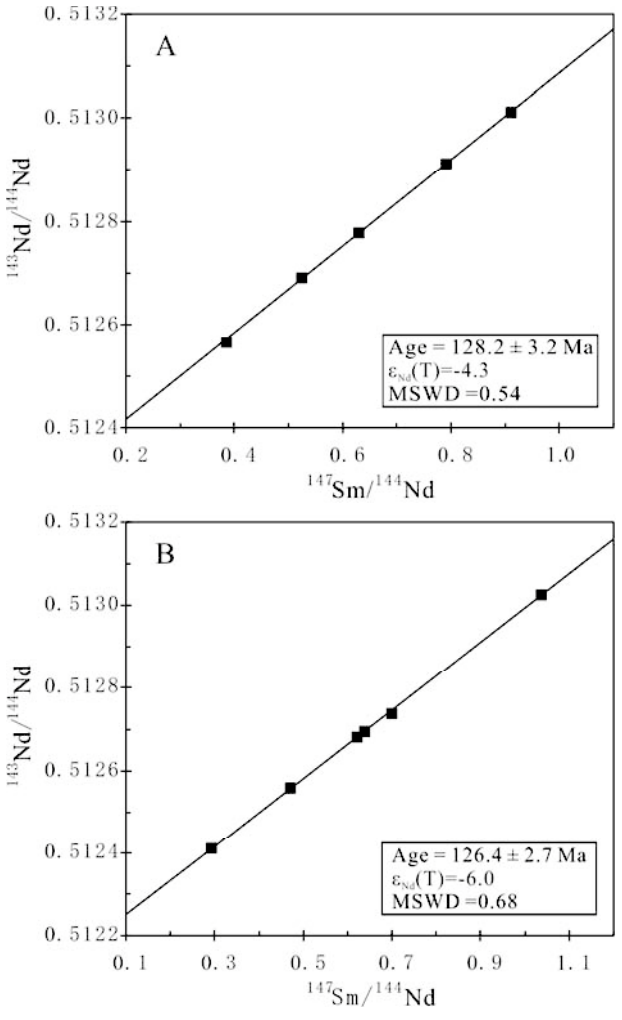

Fig. 4. Sm–Nd isochrons for the (A) white calcites and (B) pink calcites from the Banian antimony deposit.

Table. 2. Stable carbon and oxygen isotope compositions of calcites and limestones from Banian deposit

Sample No.	Sample type	$\delta^{13}C_{PDB}$ (‰)	$\delta^{18}O_{SMOW}$ (‰)	Data source
BN-6-1	White - transparent calcite	–1.8	14.6	This text
BN-11	White calcite	–1.8	14.3	″
BN-21	White calcite	–1.7	13.5	″
BN-26-1	White - transparent calcite	–0.9	12.5	″
BN-6-2	Light pink calcite	–0.5	13.7	″
BN-9-2	Light pink calcite	–0.5	12.9	″
BN-17	Light pink calcite	–0.5	13.5	″
BN-26-2	Light pink calcite	–0.6	14.0	″
BN-30	Slightly altered limestone	1.5	17.5	″
Inc-2	Calcite	–0.3	13.6	Cui and Jin, 1993
CW-12-8	Calcite	–0.1	12.3	″
bn-2	Calcite	0.1	12.1	″
bn-8	Calcite	–1.2	13.7	″

Note: $\delta^{18}O_{SMOW} = 1.03086 \cdot \delta^{18}O_{PDB} - 30.86$.

good isochron. The range of $^{147}Sm/^{144}Nd$ values of both white calcites (0.3849–0.9109) and pink calcites (0.2925–1.0366) is significantly greater, compared to those of Uysal *et al*. (2007) and Su *et al*. (2009). Therefore, such remarkable range in $^{147}Sm/^{144}Nd$ ratios, allows placing an important constraints on the timing of mineralization (Chesley *et al*., 1991, 1994; Peng *et al*., 2003a).

Sm–Nd data for five white calcite samples were plotted on an isochron, giving an age of 128.2 ± 3.2 Ma, with initial $\varepsilon_{Nd} = -4.3$ and MSWD = 0.54 (Fig. 4A); six pink calcite samples yield an isochron age of 126.4 ± 2.7 Ma, with initial $\varepsilon_{Nd} = -6.0$ and MSWD = 0.68 (Fig. 4B). Because a simple linear relationship of $1/Nd–^{143}Nd/^{144}Nd$ does not exist for the two separate groups of calcites, both isochron ages are considered to have geological significances (Tuner *et al*., 2003). However, these two ages are in good agreement within analytical errors, suggesting that they formed during the same hydrothermal event.

C and O isotopes

The carbon and oxygen isotopic composition of all Banian samples and four calcites quoted from Cui and Jin (1993) are listed in Table 2, and shown in Fig. 5. In general, white calcite is lower in $\delta^{13}C$ (–1.8‰ to –0.9‰) in comparison to the pink calcite (–0.6‰ to –0.5‰), while the $\delta^{18}O$ occurs in the reverse trend, the white calcite (12.5‰ to 14.6‰) is slightly higher than the pink calcite (12.9‰ to 14.0‰). The slightly altered limestone differs from calcites by significantly increased $\delta^{18}O$ (17.5‰) and $\delta^{13}C$ (1.5‰). A negative correlation array is defined by the $\delta^{13}C$ and $\delta^{18}O$ values of calcites.

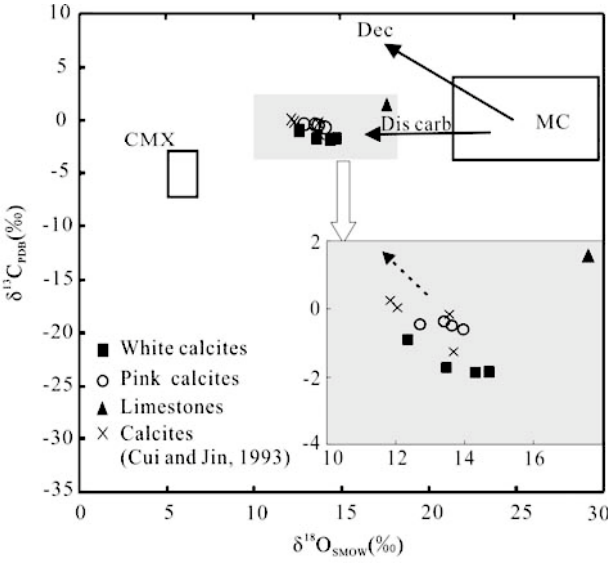

Fig. 5. The $\delta^{13}C$ versus $\delta^{18}O$ diagram for calcites and limestone from the Banian antimony deposit. For reference, the fields for typical marine carbonates (MC) and igneous carbonate rocks (CMX = carbonatite and mantle xenoliths) are outlined. The black solid line arrows represent typical isotopic trends resulting from carbonate dissolution = Dis carb, decarbonation = Dec. The dash line arrow shows a negative relationship between $\delta^{13}C$ and $\delta^{18}O$. See text for further description.

REE, Fe, Mn and Mg data of calcites and stibnites

The concentrations of REE for calcites, stibnites and wall rocks are presented in Table 3, and displayed in Fig. 6, which were normalized using the chondritic composi-

Table. 3. Rare earth element data (ppm) for calcites, stibnites and wall rocks from the Banian deposit

Sample No.	Sample characteristic	La	Ce	Pr	Nd	Sm	Eu	Gd	Tb	Dy	Ho	Er	Tm	Yb	Lu	Y	ΣREE	ΣREE+Y	LREE	HREE	LREE/HREE	δEu	Y/Ho
BN-6-1	White and transparent	<0.5	<0.5	0.03	0.30	0.58	0.34	1.8	0.43	2.8	0.56	1.4	0.18	1.0	0.16	17	9.5	27	1.3	8.3	0.15	0.94	31
BN-11	White	<0.5	<0.5	0.05	0.40	0.43	0.23	1.2	0.30	1.8	0.39	0.90	0.12	0.65	0.09	13	6.5	19	1.1	5.4	0.21	0.92	32
BN-14	Transparent	<0.5	<0.5	<0.03	0.10	0.31	0.22	1.3	0.30	1.9	0.42	1.0	0.14	0.73	0.10	14	6.5	20	0.63	5.9	0.11	0.93	32
BN-21	White	<0.5	<0.5	0.08	0.50	0.47	0.24	1.3	0.31	1.9	0.39	0.94	0.13	0.67	0.10	13	6.9	19	1.3	5.6	0.23	0.90	32
BN-26-1	White and transparent	<0.5	<0.5	0.05	0.40	0.57	0.37	2.0	0.51	3.3	0.72	1.7	0.25	1.3	0.18	22	11	33	1.4	10	0.14	0.94	31
BN-9-2	Light pink	<0.5	1.2	0.20	1.0	0.50	0.23	1.2	0.25	1.6	0.31	0.86	0.12	0.76	0.11	9.5	8.3	18	3.1	5.2	0.61	0.89	31
BN-17	Light pink	<0.5	0.50	0.09	0.60	0.50	0.25	1.4	0.31	2.0	0.38	1.0	0.13	0.73	0.10	12	8.0	20	1.9	6.1	0.32	0.84	31
BN-22	Light pink	<0.5	<0.5	0.06	0.40	0.59	0.35	1.9	0.45	2.8	0.54	1.4	0.17	0.95	0.13	18	10	28	1.4	8.4	0.17	0.91	34
BN-23	Pink	<0.5	<0.5	0.07	0.40	0.64	0.50	2.7	0.67	4.1	0.85	2.2	0.32	1.6	0.24	25	14	39	1.6	13	0.13	1.0	30
BN-26-2	Light pink	<0.5	<0.5	<0.03	0.10	0.14	0.12	0.70	0.17	1.1	0.21	0.56	0.08	0.43	0.05	6.7	3.7	10	0.36	3.3	0.11	0.95	32
BN-27	Light pink	<0.5	<0.5	0.06	0.40	0.57	0.35	1.9	0.44	2.8	0.55	1.4	0.19	1.0	0.14	17	9.8	27	1.4	8.4	0.16	0.93	32
BN-1	Stibnite	25	<0.5	<0.03	<0.1	<0.03	<0.03	<0.05	<0.01	0.11	0.01	0.03	<0.01	0.04	<0.01	<0.5	25	25	25	0.19	130		
BN-2	Stibnite	21	<0.5	<0.03	<0.1	<0.03	0.04	<0.05	<0.01	0.05	<0.01	0.03	<0.01	0.04	0.01	<0.5	21	21	21	0.13	164		
BN-3	Stibnite	15	<0.5	<0.03	<0.1	<0.03	<0.03	<0.05	<0.01	<0.05	<0.01	<0.03	<0.01	0.03	<0.01	<0.5	15	15	15	0.03	500		
BN-4	Stibnite	25	<0.5	<0.03	<0.1	<0.03	<0.03	<0.05	<0.01	0.07	0.01	<0.03	<0.01	<0.03	<0.01	<0.5	25	25	25	0.08	313		
BN-5	Stibnite	30	2.0	0.19	1.1	0.07	<0.03	<0.05	<0.01	0.10	0.01	<0.03	<0.01	<0.03	<0.01	<0.5	33	33	33	0.11	302		
BN-6	Stibnite	25	1.6	0.11	0.30	<0.03	<0.03	0.05	<0.01	0.11	0.01	0.05	<0.01	0.04	<0.01	0.5	27	28	27	0.26	105		50
BN-30	Near-ore wall rocks	7.5	14	1.8	6.5	1.1	0.19	0.71	0.14	0.84	0.19	0.50	0.07	0.40	0.06	3.4	34	37	31	2.9	11	0.61	18
BN-31	Near-ore wall rocks	16	30	3.7	14	2.8	0.48	2.4	0.57	3.2	0.70	1.9	0.25	1.54	0.20	14	78	92	67	11	6.2	0.56	20
BN-32	Near-ore wall rocks	21	37	4.4	17	3.1	0.42	1.7	0.36	1.8	0.40	1.3	0.16	1.0	0.15	8.6	89	98	82	6.9	12	0.51	22
BN-33	Near-ore wall rocks	6.0	11	1.4	4.9	0.95	0.15	0.63	0.13	0.73	0.17	0.45	0.06	0.35	0.06	3.3	27	30	24	2.6	9.4	0.55	20
BN-19	Distal wall rocks	8.7	15	2.0	8.1	1.6	0.31	1.4	0.25	1.5	0.35	0.92	0.12	0.73	0.11	6.8	41	48	35	5.4	6.6	0.62	19

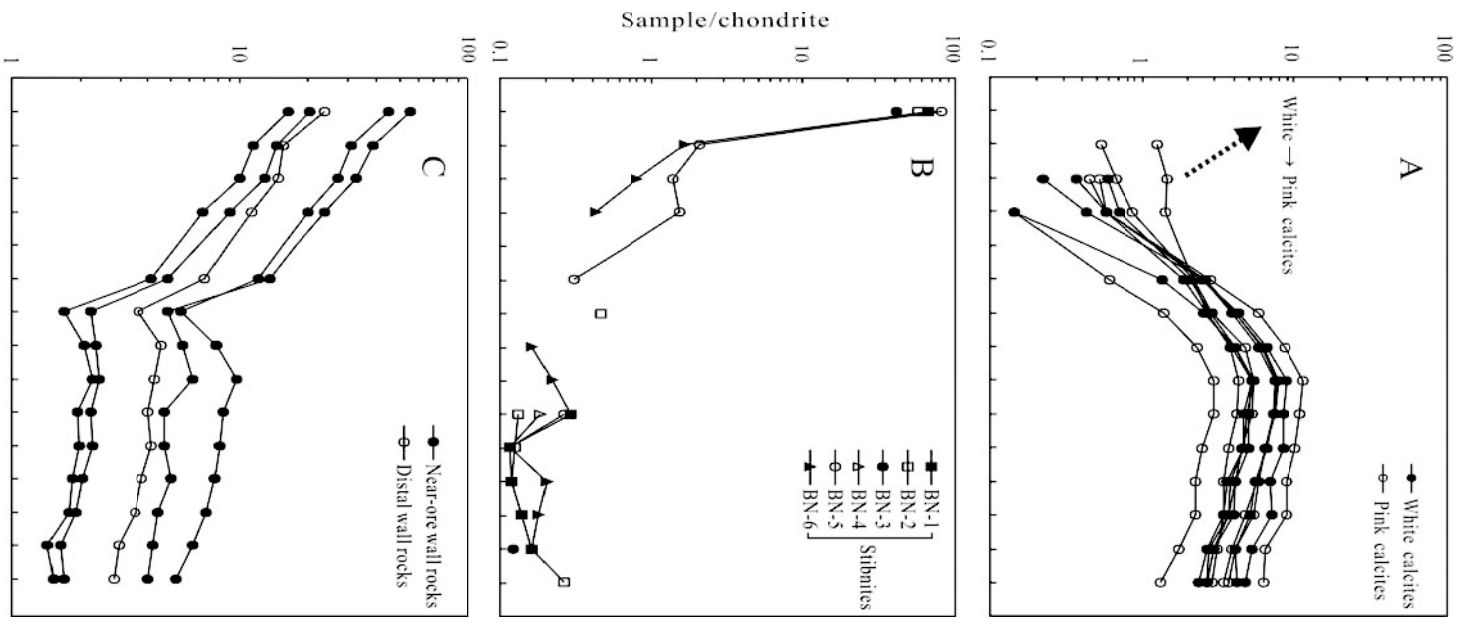

Fig. 6. A) REE patterns of white and pink calcites from the Banian deposit, arrow represents the increasing tendency of LREE from white calcite to pink calcite; B) REE patterns of stibnites; C) REE patterns of near-ore and distal wall rocks (Taylor and McLennan, 1985).

Table. 4. Fe, Mn and Mg abundances of calcites from Banian antimony deposit, Wanshan and Lae mercury deposits

Sample No.	Mg (%)	Fe (%)	Mn (ppm)
BN-6-1	0.11	0.28	511
BN-11	0.14	0.31	464
BN-26-1	0.10	0.27	609
BN-21	0.10	0.21	633
BN-14	0.10	0.32	874
BN-6-2	0.08	0.42	722
BN-9-2	0.06	0.25	727
BN-17	0.07	0.32	867
BN-22	0.08	0.33	806
BN-26-2	0.08	0.47	988
WSH-06-01	0.12	0.01	71
WSH-06-2	0.12	0.01	73
WSH-06-3	0.14	0.01	76
WSH-06-4	0.12	0.02	77
LE-11-3	0.20	<0.01	917
LE-11-8	0.22	0.01	1980
LE--11-12	0.21	0.01	274

Abbreviations: BN = Banian, WSH = Wanshan, LE = Lae.

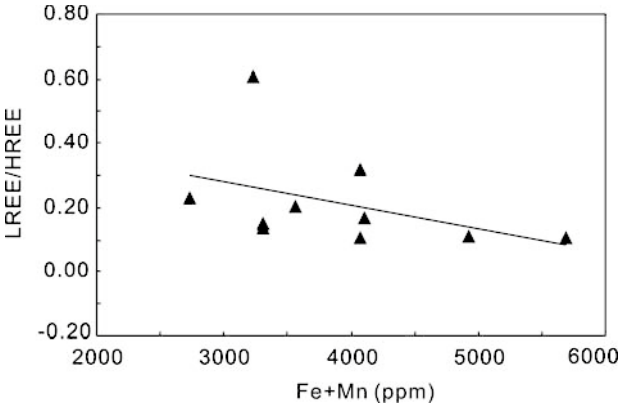

Fig. 7. The LREE/HREE versus Fe+Mn diagram for calcites from the Banian antimony deposit.

tion of Taylor and McLennan (1985).

The REE characteristics of calcites, stibnites and wall rocks are significantly different. Both types of calcites contain relatively high total REE abundances (∑REE = 3.7–14 ppm), and show significant REE fractionation with strong MREE- and HREE-enrichments and LREE-depletions. La is below detection limits (Fig. 6A). In detail, except for one sample (BN-26-2) with rather low total REE abundance (3.7 ppm), the pink calcites have higher REE abundances (8.0–14 ppm) than white calcites (6.5–11 ppm). In particular the LREE abundances of pink calcites (1.4–3.1 ppm) are higher than the white calcites (0.63–1.4 ppm), and the LREE/HREE ratios of pink calcites (0.13–0.61) are also clearly higher than white calcites (0.11–0.23). The REE abundances described above show the tendency of an increase in the LREE concentration while the concentration of HREE remains nearly constant. All of the calcite samples contain high Y content (6.7–25 ppm), with identical Y/Ho ratios (30–34).

In contrast to calcites which have strongly LREE-depleted patterns, all stibnite samples show strongly LREE-enriched patterns (Fig. 6B) with high LREE/HREE ratios (105–500). Except for high La content (15–30 ppm), abundances of other REE fall off steeply as atomic number increases (and ionic radius decreases) and, as a result, individual values of MREE and HREE for most samples are near the detection limits. Almost all of the stibnites contain Y (≦0.5 ppm) below the detection limit, which is also in contrast to the calcites.

The total REE abundances of wall rocks (∑REE = 34–89 ppm), regardless of proximity to ore, are higher in comparison to calcites or stibnites. They show moderately LREE-enriched (LREE/HREE = 6.2–12), Wright-wing-type patterns, with moderate Eu anomalies (δEu = 0.51–0.62) (Fig. 6C). The ∑HREE of wall rocks (2.6–11 ppm) are similar to calcites (3.3–13 ppm), however, with lower Y/Ho ratios (18–22) in wall rocks.

Mg, Fe and Mn contents of calcites from the Banian antimony deposit and the Wanshan and Lae mercury deposits are presented in Table 4. The calcites in the Banian deposit show a negative correlation between Fe+Mn (ppm) and LREE/HREE ratios (Fig. 7). They are nearly twenty times higher in Fe content than those of the Wanshan and Lae mercury deposits and ten times higher in Mn content than Wanshan, however, are consistent with Lae mercury deposits in Mn content. Otherwise, the Mg contents of calcites in mercury deposits are two times higher than Banian antimony deposit. Based on our present TEM (Transmission electron microscope) analyses on many individual calcite samples from Banian deposit, Fe and Mn are present as nanoparticles (<10 nm, an unknown Fe–Mn–Si–Cl–S–O? phase) in calcite crystals (Figs. 8A and B).

DISCUSSION

Sm–Nd isochron age

Numerous studies have been attempted to obtain ore-forming ages of epithermal deposits in SW China using a variety of isotopic methods (Zhang and Yang, 1992; Feng *et al*., 1993; Jia *et al*., 1993; Wei, 1993; Hu *et al*., 1996; Luo, 1997; Su *et al*., 1998; Zhu *et al*., 1998; Peng *et al*., 2003a, b; Hu *et al*., 2007a; Su *et al*., 2009). The acquired ages range from 80 to 160 Ma (Table 5), corresponding to the Yanshanian Orogeny. However, the large range of age determinations obtained by previous studies and the questionable reliability of the analytical methods remains serious impediments to constructing a clear history of

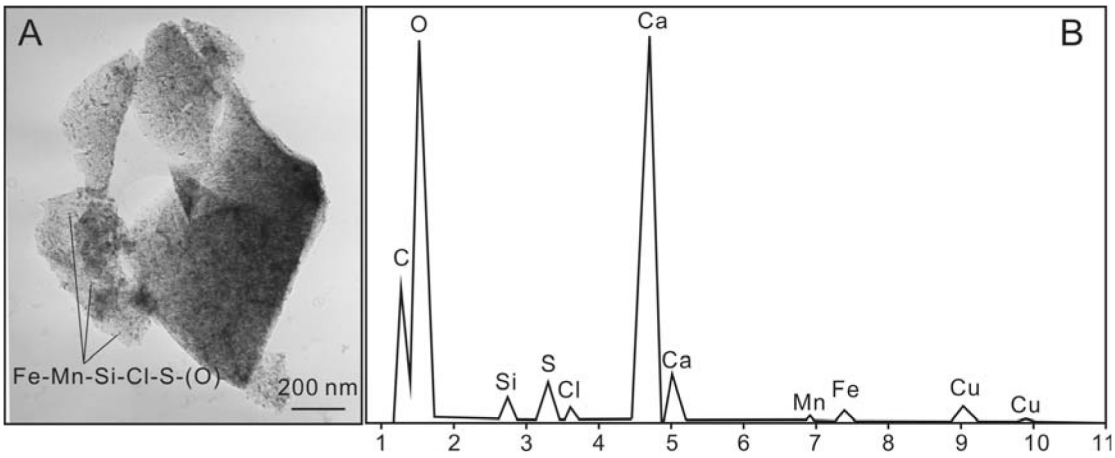

Fig. 8. A) TEM image of Fe–Mn–Si–Cl–S–(O) nanoparticle in calcites; B) EDS of nanoparticle.

Table. 5. Compilation of isotopic ages of Yanshannian mineralization from SW China

Ore types	Ore deposits	Ore-hosted strata	Test objects and methods	Age (Ma)	Referrences
Antimony ore	Xikuangshan	Devonian	Calcite, Sm–Nd isochron	155.5 ± 1.1	Peng *et al*., 2003a
				124.1 ± 3.7	
	Xikuangshan	Devonian	Calcite and stibnite, Sm–Nd isochron	156.3 ± 12.0	Hu *et al*., 1996
	Muli	Devonian	Quartz, Ar–Ar plateau age	165	Hu *et al*., 2007a
	Maxiong	Cambrian–Devonian	K–Ar	141	Wei, 1993
			Rb–Sr	156	
	Qinglong	Permian	Fluorite, ESR	104.0	Zhu *et al*., 1998
			Quartz, ESR	125.2	
	Qinglong	Permian	Fluorite, Sm–Nd isochron	148 ± 8	Peng *et al*., 2003b
				142 ± 16	
	Dushan	Devonian	Fluid inclusion, K–Ar isochron	145	Feng *et al*., 1993
Carlin-type Gold ore	Shuiyindong	Permian–Triassic	Calcite, Sm–Nd isochron	134 ± 3	Su *et al*., 2009
				136 ± 3	
	Baidi	Triassic	Quartz, Fission track	90.8 ± 6.4	Zhang and Yang, 1992
				84.5 ± 6.8	
	Lannigou	Triassic	Quartz, Fission track	82.3 ± 7.5	
				83.4 ± 8.3	
	Lannigou	Triassic	Quartz, Fluid inclusion Rb–Sr isochron	105.6	Su *et al*., 1998
	Yata	Triassic	Quartz, Fission track	100	Luo, 1997
	Danzhai	Cambrian–Lower Ordovician	Ore, Rb–Sr isochron	114 ± 6	Jia *et al*., 1993

epithermal ore formation during the Yanshannian tectonic event. Consequently, the exact ore-forming age of most epithermal deposits in SW China remain unknown. Recently, Peng *et al*. (2003a) and Su *et al*. (2009) have successively obtained precise age constraints for the Xikuangshan antimony deposit (155.5 ± 1.1 Ma, 124.1 ± 3.7 Ma) and Shuiyindong Carlin-type gold deposit (134 ± 3 Ma to 136 ± 3 Ma) situated in the region, utilizing calcite Sm–Nd chronology. These studies illustrate great potential of the method to constrain the geochronology of other epithermal deposits in SW China.

On a regional geological basis, the ore-forming ages of Banian antimony deposit presented in this paper (128.2 Ma, 126.4 Ma) are in good agreement with the age of late-stage mineralization (124.1 Ma) at the Xikuangshan deposit (Peng *et al*., 2003a), and the ore-forming ages of the Shuiyindong gold deposit (135 Ma) (Su *et al*., 2009). However, they are differentiated from the early-stage mineralization (155.5 Ma, 156.3 ± 12.0 Ma) at the Xikuangshan deposit (Peng *et al*., 2003a; Hu *et al*., 1996), and the imprecise Sm–Nd isochron ages of fluorites (148 ± 9 Ma to 142 ± 16 Ma) from the Qinglong antimony

deposit (Peng *et al*., 2003b). Therefore, two stages of antimony mineralization can be identified in the South China antimony ore belt; an early stage occurred from 155 Ma to 145 Ma, which is in the range of high-temperature W–Sn–Bi–Mo mineralization period (180–135 Ma) in Southeastern China, corresponding to the widespread magmatism caused by low-angel subduction of the Paleopacific plate (Mao *et al*., 2011). The later stage antimony mineralization occurred during the period of 130 Ma to 120 Ma, together with epithermal Au–As–Hg–U (135–80 Ma) mineralization in Southwestern China can be ascribed to regional large-scale lithospheric extension (Hu *et al*., 2007b; Mao *et al*., 2011).

In Fig. 4 of Banian calcite Sm–Nd dating, the initial ε_{Nd} values for the two regression lines are –4.3 and –6.0, respectively. The negative ε_{Nd} values indicate derivation of the rare earth elements in the fluid (and possibly the fluid itself) from crust material (Anglin *et al*., 1996). The difference existed between separate stages of calcite, probably it may resulted from progressive evolution of ore-forming fluid, the intensification of fluid/rock interaction, and the variable local sources of wall rocks (Peng *et al*., 2003b). The initial ε_{Nd} values are clearly more radiogenic compared with those of other gangue calcites from Xikuangshan antimony deposits (–15) in South China (Peng *et al*., 2003a; Hu *et al*., 1996). This indicates that the source rocks of REE and ore materials are different between Xikuangshan and Banian. In Xikuangshan, the ore materials probably originated from the Proterozoic basement (Peng *et al*., 2003a), where in Banian, they were probably originated from the Devonian limestone wall rocks, which is also supported by trace elements and isotopes studies (Cui and Jin, 1993).

C and O isotopes

In general, the calcite precipitation and C, O isotopic fractionation is mainly controlled by three mechanisms: CO_2 degassing; fluid mixing and fluid/rock interaction, respectively (Zheng, 1990; Zheng and Hoefs, 1993). The calcites from Banian are relatively homogeneous in C and O isotopic compositions, thus the fluid mixing mechanism should not be the dominant factor (Peng and Hu, 2001), which is also supported by the homogeneous Y/Ho ratios and salinities mentioned above. In addition, a clear evidence of degassing CO_2 has not been found through fluid inclusion studies (Wang and Jin, 2010), despite the absence of evidence of hydrothermal boiling which does not exclude a slow loss of CO_2 (Zheng, 1990). On the other hand, in the $\delta^{18}O$ versus $\delta^{13}C$ diagram (Hu *et al*., 2002); all samples fall in the field from dissolution of carbonate rocks, suggesting that the formation of calcites was resulted from fluid/rock interaction between meteoric water and limestone wall rocks. This conclusion is also supported by the field observation, which found that there are many vuggy open space developed in the near-ore wall rocks (Fig. 3C), suggesting a strong fluid/rock interaction may have happen in the mineralization process. Although the ranges in the C and O isotopic compositions of calcites are relatively small, a significant evolution toward a lighter O and heavier C isotopic composition with advancing crystallization is observed from early white calcites to late pink calcites, indicating the fluid changing slightly but consistently during ore formation (Fontboté and Gorzawski, 1990). And such negative correlation array between $\delta^{13}C$ and $\delta^{18}O$ values of the calcites can be best explained by the precipitation of calcite from a HCO_3^- dominant fluid in a relatively high-pH condition (Zheng, 1990), which is confirmed by the pH calculation (pH = 8.25) based on the composition of fluid inclusion (Wang and Jin, 2010).

Precipitation of calcite in an open (Eq. (1)) or closed (Eq. (2)) systems follows the reactions (Bau and Möller, 1992).

$$Ca^{2+} + CO_2 + H_2O \Leftrightarrow CaCO_3 + 2H^+ \quad (1)$$

$$Ca^{2+} + HCO_3^- \Leftrightarrow CaCO_3 + H^+. \quad (2)$$

In both reactions the solution becomes more acidic in the course of calcite precipitation, while stibnite deposition is mainly controlled by decreasing temperature and, is favored by decreasing pH (Williams-Jones and Norman, 1997). Therefore, this mechanism can also explain the phenomenon that the stibnite was the latest crystalline phase in the Banian antimony deposit.

REE and Fe, Mn

It is interesting that the calcite Sm–Nd chronology is popular and available to constrain the ore-forming ages of epithermal deposits (e.g., Peng *et al*., 2003a, b; Su *et al*., 2009). This is because the calcites in these deposits are unique for that they contain abundance of REE and show enrichment of MREE and HREE relative to LREE. But what determines the enrichment of MREE and HREE to calcite? It is important that the origins are identified.

On the whole, the LREE/HREE fractionation of hydrothermal carbonates is mainly controlled by the composition of the primary fluid, mineralogy, crystal structure, complexation, coprecipitation of an LREE (MREE or HREE)-enriched phase, and the process of sorption and desorption (Morgan and Wandless, 1980; Bau, 1991; Chesley *et al*., 1991; Bau and Möller, 1992; Subías and Fernández-Nieto, 1995; Peng *et al*., 2004; Schönenberger *et al*., 2008). In the following sections, we will briefly examine the possible processes responsible for the MREE- and HREE-enriched patterns in calcites.

In Banian, both MREE- and HREE-rich phase and LREE-rich phase has been found in the hydrothermal

minerals. Hydrothermal fluids originated from meteoric water usually have low REE concentrations (ranging from 1 to nearly 10^{-6} times chondrite) and show LREE-enriched pattern (Wood and Shannon, 2003). Carbonate wall rocks, the most possible providers of REE for the ore-fluids, no matter the near-ore or distal show a consistent REE pattern with moderate enrichment in LREE. Therefore, the primary hydrothermal fluid unlikely has such MREE- and HREE-enriched pattern like calcite, and the primary fluid should not be the major factor dominanting the REE pattern of calcite. As mentioned above, the white calcite, pink calcite and stibnite were formed one by one. The white calcite shows most enrichment of MREE and HREE and depletion of LREE, implying that the calcites should strongly prefer to incorporate MREE and HREE. With the continuous evolution of ore-fluid and precipitation of white calcite, the concentrations of MREE and HREE decreased, but the LREE relatively increased. Consequently, the late pink calcite naturally has higher LREE, compared to the early white calcite. As the fluid progressively evolved to the latest stage, the remnant fluid was extremely depleted in MREE and HREE, but relatively enriched in LREE, therefore, leading to the LREE enrichment in latest precipitated stibnite. Especially the La element, which was the last option for the calcite, was relatively enriched in the residual fluids, thus was most enriched in the latest stage mineral of stibnite. There is no crystal lattice site which could easily accommodate REE in stibnite, REE mineral inclusions in stibnite have not been found by optical and electron microscopy. However, stibnite minerals usually contain a large quantity of fluid inclusions (e.g., Luders, 1996). Therefore, we suggest that the possible occurrence of REEs in stibnite is as fluid inclusions and in lattice defects. The REE distribution in stibnite may reflect the REE patterns of the mineralizing fluids.

Morgan and Wandless (1980) suggested that the relative REE pattern in a simple hydrothermal mineral is governed by the ionic radius (mineralogical control) of the major cation. Due to the smaller differences in ionic radii between Ca^{2+} and the $LREE^{3+}$ than these between Ca^{2+} and the $HREE^{3+}$, the LREE are incorporated into the calcite crystal lattice more easily than the HREE. Therefore, calcite should have LREE-enriched pattern as usual, evidently this is not so. In addition, through construct relational graph for crustal-normalized REE patterns VS the REE ionic radius, VS the relative ionic radius and VS the relative ionic volume for the hydrothermal calcites from the Xikuangshan deposit. Peng *et al*. (2004) indicated that the optimum ion radius of substitutional site for the REE in the hydrothermal calcites from Xikuangshan is about 0.091 ± 0.001 nm, which is obviously smaller than the theoretical value (1.000 nm, CN = 6, Shannon, 1976) of the ideal Ca^{2+} ion. They contemporaneously indicated that

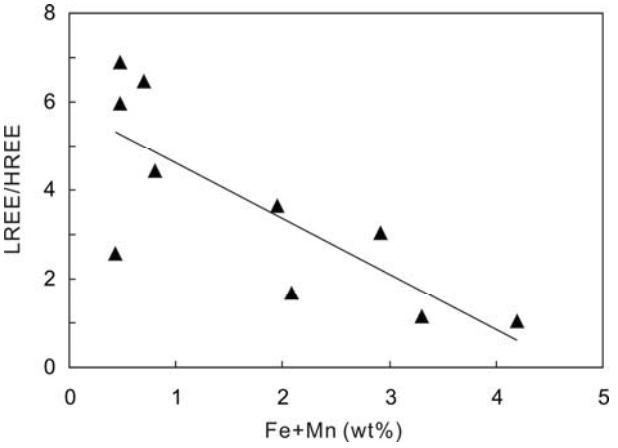

Fig. 9. The LREE/HREE versus Fe+Mn diagram for calcites from the Furong tin deposit (data from Shuang et al., 2010).

the optimum site in the hydrothermal calcites is determined by the crystal structure of calcite rather than by the Ca^{2+} ion in calcites. However, they didn't show the differences of crystal structure between MREE- and HREE-enriched calcites and those LREE-enriched calcites. Alternatively, the LREE-depleted pattern should be controlled by complexation processes, due to the ligand-enriched fluid (Bau, 1991; Bau and Möller, 1992; Subías and Fernández-Nieto, 1995). In case the above complexation mechanism is taken to be responsible for such fractionation in Banian, owing to REE complexation with ligands like CO_3^{2-} and OH^- which form more stable complexes with the HREE. Therefore, LREE preferentially precipitate in the early stage, and the late stage fluid should be HREE-enriched (Möller *et al*., 1976). However, it is conflicting to the characteristics in Banian, where the latest stage of stibnite is enriched in LREE, especially in La element. Chesley *et al*., (1991) suggested that the most likely mechanism for producing LREE-depleted pattern of fluorites from SW England is the coeval precipitation of an unidentified LREE-enriched phase. In Banian, we have found that stibnite mineral is the LREE-enriched phase, but it crystallized later than calcite. Moreover, it is well known that the REE can hardly incorporate into the crystal lattice of stibnite minerals, thus this hypothesis is also precluded.

In addition to the above mechanisms, it is suggested that the REE fractionation processes are the results of two basic steps of sorption of REE onto and desorption from particle surfaces during migration of a REE-bearing fluid and coprecipitation (Bau and Möller, 1992). Similarly, Johannesson and Lyons (1995) reported that the dissolution of MREE-enriched suspended particles and/or coatings on the sedimentary rocks within the Colour Lake basin may be responsible for the MREE enrichments of

Colour Lake water. In addition, the secondary minerals associated with aquifer materials may also contribute to the MREE enrichment of groundwaters and lake waters (Johannesson *et al*., 1996).

The Fe and Mn contents of calcites from the Banian antimony deposit are apparently higher than those of LREE-enriched calcites from the Wanshan (Wang *et al*., 2010) and Lae (unpublished data) mercury deposits, and are also several magnitudes higher than REE content. Furthermore, the negative relationship between Fe+Mn (ppm) and LREE/HREE ratios of calcites in the Banian deposit also clearly indicates that the higher Fe+Mn concentrations correspond to the lower LREE concentrations and the higher HREE concentrations. Many previous studies have displayed that the Fe–Mn-bearing phase can be enriched in the MREE and HREE by sorption, such as hydrogenetic Fe–Mn crust (Bau *et al*., 1996), Fe-rich organic colloids, Fe–Mn surface coatings or suspended particles (Palmer, 1985; Palmer and Elderfield, 1986; Johannesson *et al*., 1996), Mn crust (Alt, 1988), Fe–Mn ores (Kato *et al*., 2005; Brugger and Meisser, 2006). Furthermore, according to the foraminifera and seawater studies, it is suggested that the Fe–Mn-rich coating phase has significantly higher REE concentrations than their lattice phase (Palmer, 1985; Palmer and Elderfield, 1986; Banner *et al*., 1988).

The Fe and Mn are present as nanoparticles in the calcite crystals in Banian deposit. Therefore, regardless of the exact mechanism, it is reasonable that the Fe–Mn nanoparticle impurities may play an important role on the enrichment of MREE and HREE in calcites. This inference is also evidenced by Shuang *et al*. (2010), which reported three types of calcites present in the Furong tin deposit, and a negative relationship also occurs between Fe+Mn (wt%) and LREE/HREE ratios (Fig. 9). However, more work is required, to verify or refute these mechanisms and to examine, in detail, the significance of Fe–Mn impurities, in the development of MREE and HREE in calcites.

Though HREE may prefer to incorporate into the Fe–Mn nanoparticle impurities within calcite, they were precipitated with calcite crystals simultaneously, thus the REE isotope information in the Fe–Mn impurities are consistent with that in the crystal lattice of calcites. Cherniak (1998) suggested that the REE diffusion in calcite is very slow, even during diffusive alteration, REE isotope and chemical information in calcite is quite possibly preserved. In addition, no tectonic event occurred after the Yanshanian Sb mineralization in the region, the influence of thermal disturbance on the calcites from the Banian deposit is probably negligible. Thus, Sm–Nd isotopic systematics in the calcites from the Banian deposit should have been closed and preserved initial information of the mineralization; the isochron ages of the calcites should represent the timing of the coeval antimony mineralization (Peng *et al*., 2003a).

Conclusion

(1) There are two types of white and pink calcites in the Banian antimony deposit, corresponding to two ages of 128.2 ± 3.2 Ma and 126.4 ± 2.7 Ma, respectively. These two ages are in good agreement within analytical uncertainty. And they are the first reported ore-forming ages for Banian deposit, corresponding to the late stage of antimony mineralization in South China and the late stage of Yanshanian orogeny.

(2) The $\delta^{18}O$, $\delta^{13}C$, initial ε_{Nd} values, together with field evidence of abundance of vuggy open spaces, all suggest that the ore-forming fluid originated from dissolution of carbonate wall rocks.

(3) Both white and pink calcites show strongly LREE-depleted, MREE- and HREE-enriched REE pattern, and the late-stage pink calcite is slightly richer in LREE than the early white calcite. In contrast, the latest stibnite displays amazing enrichment of LREE, especially for La element. Those REE patterns are believed to be resulted from that calcites preferentially incorporate MREE and HREE. Subsequently, the latest residual fluid is extremely depleted in MREE and HREE but relatively enriched in LREE, leading to the late stage of stibnite enriched in LREE with no choice.

(4) The Fe–Mn impurities in calcite may play an important role on the enrichment of MREE and HREE in calcites. However, Sm–Nd isotopic systematics in calcites can still preserve initial information of the mineralization.

Acknowledgments—We are grateful to Mrs. Hui Liu (Tianjin Institute of Geology and Mineral Resources, CAGS) for Sm–Nd analysis, Mrs. Bin Wang (ALS Minerals Division) for REE, Mg, Fe and Mn analyses, Mr. Ning An, Mr. Longnian Geng and Prof. Shirong Liu (Institute of Geochemistry, Chinese Academy of Sciences, Guiyang) for C, O isotope and TEM analysis. Special thanks to Prof. Yuzhuo Qiu for fruitful discussion and improvement of the manuscript. This project was financially supported by the National Basic Research Program of China (Grant No. 2007CB411402), National Natural Science Foundation of China (Grant No. 40930425) and the 12th Five-Year Plan project of State Key Laboratory of Ore-deposit Geochemistry, Chinese Academy of Sciences (SKLODG-ZY125-07).

References

Alt, J. C. (1988) The chemistry and sulfur isotope composition of massive sulfide and associated deposits on Green Seamount, eastern Pacific. *Econ. Geol.* **83**, 1026–1033.

An, F. and Zhu, Y. F. (2010) Native antimony in the Baogutu gold deposit (west Junggar, NW China): Its occurrence and

origin. *Ore Geol. Rev.* **37**, 214–223.

Anglin, C. D., Jonasson, I. R. and Franklin, J. M. (1996) Sm–Nd dating of scheelite and tourmaline: Implications for the genesis of Archean gold deposits, Val d'Or, Canada. *Econ. Geol.* **91**, 1372–1382.

Banner, J. L., Hanson, G. N. and Meyers, W. J. (1988) Rare-earth element and Nd Isotopic variations in regionally extensive dolomites from the Burlington–Keokuk Formation (Mississippian): implications for REE mobility during carbonate diagenesis. *J. Sediment. Petrol.* **58**, 415–432.

Bau, M. (1991) Rare-earth element mobility during hydrothermal and metamorphic fluid-rock interaction and the significance of the oxidation state of europium. *Chem. Geol.* **93**, 219–230.

Bau, M. and Möller, P. (1992) Rare earth element fractionation in metamorphogenic hydrothermal calcite, magnesite and siderite. *Mineral. Petrol.* **45**, 231–246.

Bau, M., Koschinsky, A., Dulski, P. and Hein, J. R. (1996) Comparison of the partitioning behaviours of yttrium, rare earth elements, and titanium between hydrogenetic marine ferromanganese crusts and seawater. *Geochim. Cosmochim. Acta* **60**, 1709–1725.

Bell, K., Anglin, C. D. and Franklin, J. M. (1989) Sm–Nd and Rb–Sr isotope systematics of scheelites: possible implications for the age and genesis of vein-hosted gold deposits. *Geology* **17**, 500–504.

Brugger, J. and Meisser, N. (2006) Manganese-rich assemblages in the Barrhorn unit, Turtmanntal, central Alps, Switzerland. *Can. Mineral.* **44**, 229–248.

Chen, G. D. (1992) *New Development of the Diwa Theory*. Science Press, Beijing, 314 pp. (in Chinese with English abstract).

Cherniak, D. J. (1998) REE diffusion in calcite. *Earth Planet. Sci. Lett.* **160**, 273–287.

Chesley, J. T., Halliday, A. N. and Scrivener, R. C. (1991) Samarium–Neodymium direct dating of fluorite mineralization. *Science* **252**, 949–951.

Chesley, J. T., Halliday, A. N., Kyser, T. K. and Spry, P. G. (1994) Direct dating of MVT mineralization: Use of Sm–Nd in fluorite. *Econ. Geol.* **89**, 1192–1199.

Cui, Y. L. and Jin, S. C. (1993) The genesis of ore materials studies in Banian antimony deposit, Dushan. *Southwest Mineral Resources and Geology*, 21–26 (in Chinese).

Cui, Y. L., Wang, X. K. and Jin, S. C. (1993) The ore-controlling condition and mineralization enrichment mechanism studies in Dushan antimony deposit. *Southwest Mineral Resources and Geology*, 18–25 (in Chinese).

Darbyshire, D. P. F., Pitfield, P. E. J. and Campbell, S. D. G. (1996) Late Archean and Early Proterozoic gold–tungsten mineralization in the Zimbabwe Archean craton: Rb–Sr and Sm–Nd isotope constraints. *Geology* **24**, 19–22.

Eichhorn, R., Häll, R., Jagoutz, E. and Schärer, U. (1997) Dating scheelite stages: A strontium, neodymium, lead approach from the Felbertal tungsten deposit, Central Alps, Austria. *Geochim. Cosmochim. Acta* **61**, 5005–5022.

Fan, D. L., Zhang, T. and Ye, J. (2004) The Xikuangshan Sb deposit hosted by the Upper Devonian black shale series, Hunan, China. *Ore Geol. Rev.* **24**, 121–133.

Feng, Y. X., Chen, M. Y. and Xu, W. X. (1993) Stable isotope geochemistry research of Dushan antimony ore deposit. *Mineral Resources and Geology* **7**, 119–126 (in Chinese with English abstract).

Fontboté, L. and Gorzawski, H. (1990) Genesis of the Mississippi Valley-Type Zn–Pb deposit of San Vicente, central Peru: geologic and isotopic (Sr, O, C, S, Pb) evidence. *Econ. Geol.* **85**, 1402–1437.

Graf, J. L. (1984) Effects of Mississippi Valley-type mineralization on REE patterns of carbonate rocks and minerals, Viburnum trend, Southeast Missouri. *J. Geol.* **92**, 307–324.

Halliday, A. N., Shepherd, T. J., Dicken, A. P. and Chesley, J. T. (1990) Sm–Nd evidence for the age and origin of a Mississippi Valley Type ore deposit. *Nature* **344**, 54–56.

Hu, R. Z., Su, W. C., Bi, X. W., Tu, G. Z. and Hofstra, A. H. (2002) Geology and geochemistry of Carlin-type gold deposits in China. *Miner. Deposita* **37**, 378–392.

Hu, R. Z., Peng, J. T., Ma, D. S., Su, W. C., Shi, C. H., Bi, X. W. and Tu, G. Z. (2007a) Epoch of large-scale low-temperature mineralizations in southwestern Yangtze massif. *Mineral Deposits* **26**, 583–596 (in Chinese with English abstract).

Hu, R. Z., Bi, X. W., Peng, J. T., Liu, S., Zhong, H., Zhao, J. H. and Jiang, G. H. (2007b) Some problems concerning relationship between Mesozoic–Cenozoic lithospheric extension and uranium metallogenesis in South China. *Mineral Deposits* **26**, 139–152 (in Chinese with English abstract).

Hu, X. W., Pei, R. F. and Zhou, S. (1996) Sm–Nd dating for antimony mineralization in the Xikuangshan deposit, Hunan, China. *Resour. Geol.* **46**, 227–231.

Jia, R. F., Chen, Q. N., Zhou, P. K., Xia, Y. and Wu, X. Y. (1993) Relation between Au-enrichment periods and organic matter in Danzhai gold deposit, Guizhou. *Cont. Geol. Min. Resour. Res.* **8**, 69–81 (in Chinese with English abstract).

Jiang, S. Y., Slack, J. F. and Palmer, M. R. (2000) Sm–Nd dating of the giant Sullivan Pb–Zn–Ag deposit, British Columbia. *Geology* **28**, 751–754.

Jin, Z. G. and Dai, T. G. (2007) A discussion on the geological and geochemical characteristics and metallogenic model of the Banpo antimony orefield in Dushan, Guizhou province. *Geophysical and Geochemical Exploration* **31**, 129–132 (in Chinese with English abstract).

Johannesson, K. H. and Lyons, W. B. (1995) REE-earth element geochemistry of Colour Lake, an acidic freshwater lake on Axel Heiberg Island, Northwest Territories, Canada. *Chem. Geol.* **119**, 209–223.

Johannesson, K. H., Lyons, W. B., Yelken, M. A., Gaudette, H. E. and Stetzenbach, K. J. (1996) Geochemistry of rare-earth elements in hypersaline and dilute acidic natural terrestrial waters: complexation behaviour and middle rare-earth element enrichment. *Chem. Geol.* **133**, 124–144.

Kato, Y., Fujinaga, K., Nozaki, T., Osawa, H., Nakamura, K. and Ono, R. (2005) Rare earth, major and trace elements in the Kunimiyama ferromanganese deposit in the northern Chichibu belt, central Shikoku, Japan. *Resour. Geol.* **55**, 291–299.

Krupp, R. E. (1988) Solubility of stibnite in hydrogen–sulfide solutions, speciation, and equilibrium-constants, from 25 to 350°C. *Geochim. Cosmochim. Acta* **52**, 3005–3015.

Luders, V. (1996) Contribution of infrared microscopy to fluid

inclusion studies in some opaque minerals (wolframite, stibnite, bournonite): Metallogenic implications. *Econ. Geol. Bull. Soc.* **91**, 1462–1468.

Ludwig, K. (2005) Isoplot/Ex, version 3.23: A Geochronological Toolkit for Microsoft Excel. Geochronology Center, Berkeley, U.S.A.

Luo, X. H. (1997) Analysis of gold mineralization in southwestern Guizhou Based on structural styles. *Guizhou Geology* **14**, 312–320 (in Chinese with English abstract).

Mao, J. W., Pirajno, F. and Cook, N. (2011) Mesozoic metallogeny in East China and corresponding geodynamic settings—An introduction to the special issue. *Ore Geol. Rev.* **43**, 1–7.

McCrea, J. M. (1950) On the isotopic chemistry of carbonates and a paleotemperature scale. *J. Chem. Phys.* **18**, 849–857.

Möller, P., Parekh, P. P. and Schneider, H. J. (1976) The application of Tb/Ca–Tb/La abundance ratios to problems of fluorspar genesis. *Miner. Deposita* **11**, 111–116.

Morgan, J. W. and Wandless, G. A. (1980) Rare earth elements in some hydrothermal minerals: evidence for crystallographic control. *Geochim. Cosmochim. Acta* **44**, 973–980.

Obolensky, A. A., Gushchina, L. V., Borisenko, A. S., Borovikov, A. A. and Pavlova, G. G. (2007) Antimony in hydrothermal processes: solubility, conditions of transfer, and metal-bearing capacity of solutions. *Russ. Geol. Geophys.* **48**, 992–1001.

Palmer, M. R. (1985) Rare earth elements in foraminifera tests. *Earth Planet. Sci. Lett.* **73**, 285–298.

Palmer, M. R. and Elderfield, H. (1986) Rare earth elements and neodymium isotopes in ferromanganese oxide coatings of Cenozoic foraminifera from the Atlantic Ocean. *Geochim. Cosmochim. Acta* **50**, 409–417.

Peng, B. and Frei, R. (2004) Nd–Sr–Pb isotopic constraints on metal and fluid sources in W–Sb–Au mineralization at Woxi and Liaojiaping (Western Hunan, China). *Miner. Deposita* **39**, 313–327.

Peng, J. T. and Hu, R. Z. (2001) Metallogenic epoch and metallogenic tectonic environment of antimony deposits, south China. *Geology-Geochemistry* **29**, 104–108 (in Chinese with English abstract).

Peng, J. T., Hu, R. Z. and Burnard, P. G. (2003a) Samarium–neodymium isotope systematics of hydrothermal calcites from the Xikuangshan antimony deposit (Hunan, China): the potential of calcite as a geochronometer. *Chem. Geol.* **200**, 129–136.

Peng, J. T., Hu, R. Z. and Jiang, G. H. (2003b) Samarium–neodymium isotope system of fluorites from the Qinglong antimony deposit, Guizhou Province: constraints on the mineralizing age and ore-forming minerals' sources. *Acta Petrol. Sinica* **19**, 785–791 (in Chinese with English abstract).

Peng, J. T., Hu, R. Z., Qi, L., Zhao, J. H. and Fu, Y. Z. (2004) REE distribution pattern for the hydrothermal calcites from the Xikuangshan antimony deposit and its constraining factors. *Geol. Rev.* **50**, 25–32 (in Chinese with English abstract).

Pokrovski, G. S., Borisova, A. Y., Roux, J., Hazemann, J. L., Petdang, A., Tella, M. and Testemale, D. (2006) Antimony speciation in saline hydrothermal fluids: A combined X-ray absorption fine structure spectroscopy and solubility study. *Geochim. Cosmochim. Acta* **70**, 4196–4214.

Roberts, S., Palmer, M. R. and Waller, L. (2006) Sm–Nd and REE characteristics of tourmaline and scheelite from the Björkdal Gold Deposit, Northern Sweden: Evidence of an intrusion-related gold deposit? *Econ. Geol.* **101**, 1415–1425.

Schönenberger, J., Köhler, J. and Markl, G. (2008) REE systematics of fluorides, calcite and siderite in peralkaline plutonic rocks from the Gardar Province, South Greenland. *Chem. Geol.* **247**, 16–35.

Shannon, R. D. (1976) Revised effective ionic radii and systematic studies of interatomic distances in halides and chalcogenides. *Acta Crystall. A-Crys.* **32**, 751–767.

Shuang, Y., Bi, X. W., Hu, R. Z., Peng, J. T., Li, H., Li, D. H. and Zhu, C. S. (2010) REE, Mn, Fe, Mg and C, O isotopic geochemistry of calcites from Furong tin deposit, south China: evidence for the genesis of the hydrothermal ore-forming fluids. *Resour. Geol.* **60**, 18–34.

Su, W. C., Yang, K. Y., Hu, R. Z. and Chen, F. (1998) Fluid inclusion chronological study of the Carlin-Type gold deposits in southwestern China: As exemplified by the Lannigou gold deposit, Guizhou province. *Acta Mineral. Sinica* **18**, 359–362 (in Chinese with English abstract).

Su, W. C., Hu, R. Z., Xia, B., Xia, Y. and Liu, Y. P. (2009) Calcite Sm–Nd isochron age of the Shuiyindong Carlin-type gold deposit, Guizhou, China. *Chem. Geol.* **258**, 269–274.

Subías, I. and Fernández-Nieto, C. (1995) Hydrothermal events in the Valle de Tena (Spanish Western Pyrenees) as evidenced by fluid inclusions and trace-element distribution from fluorite deposits. *Chem. Geol.* **124**, 267–282.

Taylor, S. R. and McLennan, S. M. (1985) *The Continental Crust: Its Composition and Evolution*. Blackwell Scientific Publications, London, 312 pp.

Turner, W. A., Heaman, L. M. and Creaser, R. A. (2003) Sm–Nd fluorite dating of Proterozoic low-sulfidation epithermal Au–Ag deposits and U–Pb zircon dating of host rocks at Mallery Lake, Nunavut, Canada. *Earth Sci.* **40**, 1789–1804.

Uysal, I. T., Zhao, J. X., Golding, S. D., Lawrence, M. G., Glikson, M. and Collerson, K. D. (2007) Sm–Nd dating and rare-earth element tracing of calcite: Implications for fluid-flow events in the Bowen Basin, Australia. *Chem. Geol.* **238**, 63–71.

Wang, J. S., Wen, H. J. and Shi, S. H. (2010) Characteristics and implications of REE, carbon and oxygen isotopes of hydrothermal calcite from the mercury metallogenic belt in Hunan and Guizhou Provinces, China. *Acta Mineral. Sinica* **30**, 185–193 (in Chinese with English abstract).

Wang, Y. L. and Jin, S. C. (2010) Geochemistry characteristics comparison of inclusion in Banpo and Banian antimony deposit of Guizhou. *Nonferrous Metals* **62**, 123–128 (in Chinese with English abstract).

Wei, W. Z. (1993) Geological features of Maxiong Sb deposit. *Mineral Resources in Southwestern China*, 8–16 (in Chinese with English abstract).

Williams-Jones, A. E. and Norman, C. (1997) Controls of mineral parageneses the System Fe–Sb–S–O. *Econ. Geol.* **92**, 308–324.

Wood, S. A. and Shannon, W. M. (2003) Rare-earth elements in geothermal waters from Oregon, Nevada, and California. *J. Solid State Chem.* **171**, 246–253.

Xiao, Q. M., Zeng, D. R., Jin, F. Q., Yang, M. Y. and Yang, Z. F. (1992) Time-space distribution feature and exploration guide of Chinese Sb-deposits. *Geology and Prospecting* **28**, 9–14 (in Chinese with English abstract).

Zhang, F. and Yang, K. Y. (1992) Fission-track ages of micro-disseminated gold deposits in Southwestern Guizhou. *Chinese Science Bulletin*, 1593–1595 (in Chinese).

Zheng, Y. F. (1990) Carbon–oxygen isotopic covariation in hydrothermal calcite during degassing of CO_2. *Miner. Deposita* **25**, 246–250.

Zheng, Y. F. and Hoefs, J. (1993) Carbon and oxygen isotopic covariations in hydrothermal calcites. *Miner. Deposita* **28**, 79–89.

Zhu, L. M., Liu, X. F., Jin, J. F. and He, M. Y. (1998) The study of the time-space distribution and source of ore-forming fluid for the fine-disseminated gold deposits in the Yunnan–Guizhou–Guangxi area. *Scientia Geologica Sinica* **33**, 463–474 (in Chinese with English abstract).